

1,8-Octanediamine Dihydroiodide-Mediated Grain Boundary and Interface Passivation in Two-Step-Processed Perovskite Solar Cells

Heng Liu, Xingnan Qi, Jiantao Wang, Weihai Zhang, Yu Xia, Yueqing Shi, Rui Chen, and Hsing-Lin Wang*

Two-step-processed perovskite solar cells show superior reproducibility in terms of stepwise crystallization management. However, the device performance is limited due to the buried-interface defects that are highly dependent on the diffusion process of organic salts into PbI_2 . Herein, 1,8-octanediamine dihydroiodide (ODADI) is adopted to develop an alkylammonium predeposition strategy for the high-quality perovskite film. It is found that the pre-deposited ODADI layer not only facilitates the diffusion of organic salts via interaction with PbI_2 , but also passivates the buried-interface defects, resulting in a perovskite film with low defect density, high crystallinity, and superior electronic properties. Consequently, the fabricated devices deliver a significant enhancement on power conversion efficiency (PCE) from 19.87 to 22.07%. In addition, a superior long-term stability in glovebox atmosphere, maintaining 96% of the initial PCE after 1000 h, is demonstrated.

obtained a stunning power conversion efficiency (PCE) of up to 25.5%,^[6] which is comparable with the commercially available silicon (Si)^[7] and copper indium gallium selenide (CIGS) solar cells.^[8,9] In addition, its low-cost precursor and solution-based fabrication enable them as one of the most promising candidates to be commercialized. Currently, the highest efficiency of one-step solution-processed PSCs is achieved using the antisolvent-assisted fast-crystallization method. This type of one-step method is atmosphere dependent and has less-than-ideal reproducibility. In contrast, the two-steps' sequential deposition separately manages the solution deposition and film crystallization that enable control growth of homogeneous films. This is a relatively effective way to obtain PSCs with more repeatable performance.^[10–12]

1. Introduction

Perovskite solar cells (PSCs) have been achieving rapid progress due to the superior semiconducting properties of perovskite materials. It is advantageous because of their tunable bandgap with a diverse range of compositions, a wide and strong absorption region, weak exciton binding energy, superior carrier mobility, and long carrier diffusion lifetime.^[1–5] Recently, PSCs have

To date, the performance of two-step-processed PSCs is still far behind that of the one-step method. The PCE is lower due to the presence of defects in the perovskite grain boundaries and interfaces.^[13–15] Lots of research has been reported on the investigation of the highly crystalline film formation and its post-treatment, to passivate the interface for the improved device performance.^[16–20] You and co-workers optimized the PbI_2 content and developed the PEAI top-surface passivation route.^[21,22] In contrast, Lu et al. doped the A-site of perovskite by incorporating GA^+ and reported high-crystalline perovskite films with high efficiency.^[23] However, very little research is focused on the buried interface modulation that not only directly influences the growth of perovskite but also has more interfacial defects in terms of downward growth of the perovskite film. Recently, Jen et al. showed that nonradiative recombination at the buried interface has a dominant impact on the device performance in one-step-processed PSCs. Furthermore, they demonstrated that the V_{oc} in PSCs can be improved from 1.12 to 1.21 eV via 1,4-butanediammonium iodide (BDAI) alkyl diammonium passivation.^[24] Zheng et al. reported that alkylamine ligands with a longer chain length should have better passivation effects, suppressing nonradiative carrier recombination that consequently improves the optoelectronic properties of perovskite films.^[25] Therefore, the tailored long alkyl diammonium is effective to be used in planar regular PSCs as buried interlayers that passivate both interfacial and grain boundary defects.

H. Liu

School of Materials Science and Engineering
Harbin Institute of Technology
Harbin 150001, China


H. Liu, X. Qi, J. Wang, W. Zhang, Y. Xia, H.-L. Wang
Department of Materials Science and Engineering
Southern University of Science and Technology
Shenzhen 518055, Guangdong, China
E-mail: wangxl3@sustech.edu.cn

Y. Shi, R. Chen

Department of Electrical and Electronic Engineering
Southern University of Science and Technology
Shenzhen 518055, Guangdong, China

Y. Xia

School of Physics and Astronomy
University of Birmingham
Birmingham B15 2TT, UK

 The ORCID identification number(s) for the author(s) of this article can be found under <https://doi.org/10.1002/solr.202100960>.

DOI: 10.1002/solr.202100960

In this work, 1,8-octanediamine dihydroiodide (ODADI) was adopted to develop an alkylammonium predeposition strategy for highly efficient two-step-processed PSCs. It is found that the bottom ODADI layer not only facilitates organic salts' diffusion via interaction with PbI_2 , thus regulating the growth process of the perovskite film, but also passivates buried-interface defects, delivering perovskite film with improved crystallinity, reduced defect density, and suppressed nonradiative recombination. Consequently, the fabricated devices show a champion PCE of 22.07%, which is much higher than its control counterpart (19.87%). In addition, the resulting device shows superior long-term (96% of its initial PCE after 1000 h) as well as thermal (over 90% of its original PCE after 800 h at 85 °C) stability.

2. Results and Discussion

The conventional two-step method has been used to fabricate perovskite films.^[1] In simple terms, the PbI_2 layer was deposited before the coating of an isopropyl alcohol (IPA) solution,

containing organic salts (FAI: MABr: MAcl) and then the resulting film was heated at 150 °C for crystallization.^[17] Herein, ODADI was introduced and predeposited on SnO_2 substrate prior to spin coating of PbI_2 (Figure 1a). The optimal concentration of ODADI is about 20 mg mL⁻¹, based on the device performance measurements (Figure S1, Supporting Information). For simplicity, the following measurements involving ODADI are based on the optimal condition, unless otherwise stated.

To study the effect of ODADI molecules on the crystal structure and surface morphology of perovskite films, X-ray diffraction (XRD), scanning electron microscopy (SEM), and atomic force microscopy (AFM) measurements were conducted. The XRD spectra of perovskite films with and without ODADI are compared and the results are shown in Figure S2, Supporting Information. Diffraction peaks at 13.9°, 24.3°, and 28.1° are assigned to the (110), (202), and (220) crystal planes of α -FAPbI₃, and the peak at 12.6° belongs to PbI_2 .^[13] However, moderately excess PbI_2 is believed to passivate the perovskite defects significantly, thus enhancing device performance and stability as reported by You and co-workers,^[22] in which they showed that

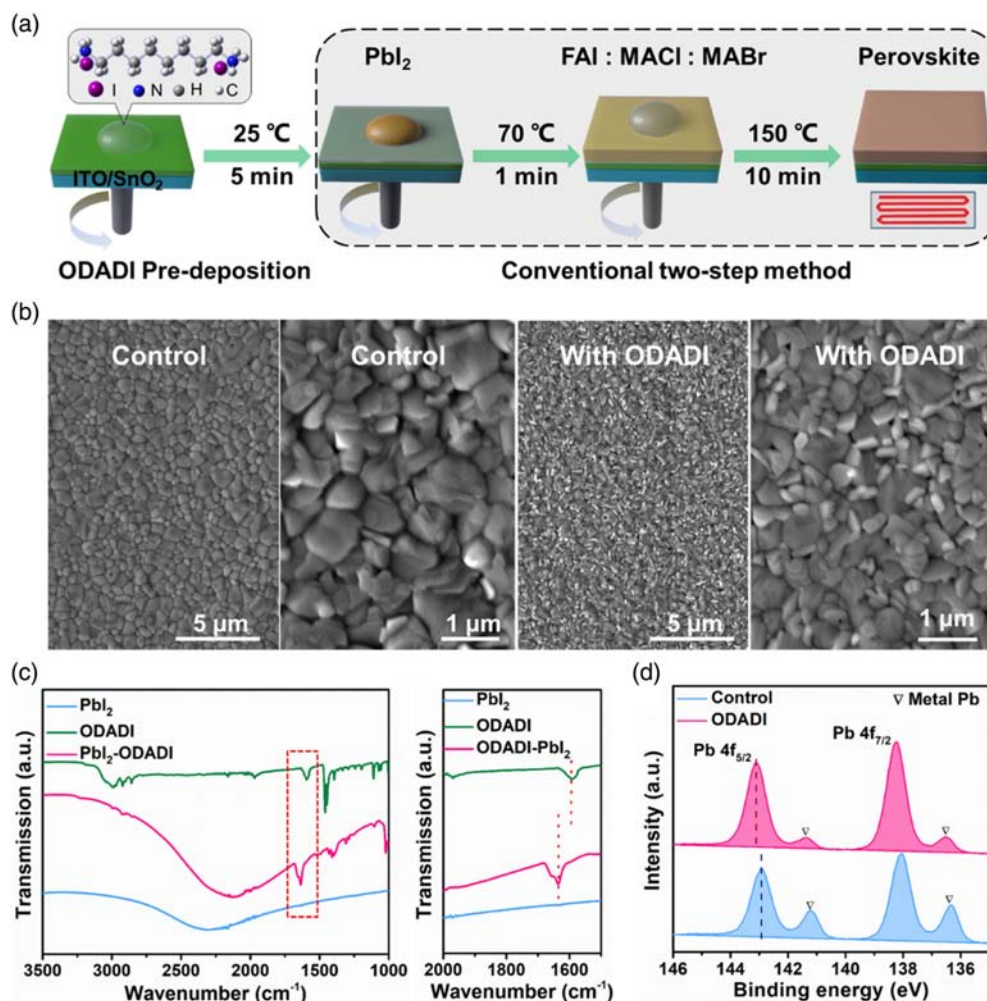


Figure 1. a) Schematic diagram for the preparation of perovskite films. ODADI was predeposited before the conventional two-step method. b) SEM images of perovskite surfaces with and without ODADI layer, respectively. c) FTIR spectra of PbI_2 , ODADI, and PbI_2 -ODADI films and their partial enlarged detail. d) XPS spectra of Pb 4f in perovskite films with and without ODADI.

the diffraction peak of residual PbI_2 is stronger than perovskite. The XRD patterns of perovskite films show no impurity phases other than PbI_2 , indicating that ODADI molecules have not been incorporated into perovskite lattice site. To confirm this, we performed XRD characterization of PbI_2 films with different ODADI concentrations, as shown in Figure S3, Supporting Information, and little difference can be observed. The existence of ODADI did not result in a noticeable peak shift toward lower angles, indicating no significant unit cell expansion in the perovskite lattice or incorporation of ODADI into the perovskite crystal structure. Figure 1b shows the SEM images of different perovskite films; it can be seen that all perovskite films are dense and pinhole free. Interestingly, with the introduction of ODADI molecules, the average grain size decreased from 800 (control perovskite film) to 500 nm, which is mainly attributed to the fast growth of perovskite film induced by the interaction between ODADI and PbI_2 . Similarly, AFM images confirmed the coincident surface morphology of perovskite films with and without ODADI. The ODADI-modified perovskite film has a root mean square (RMS) value of 18.4 nm, while that of the control film is 20.5 nm (Figure S4, Supporting Information). This indicates that the ODADI-based perovskite film has a more uniform top surface, leading to a better interface contact with the HTL layer, which could potentially enhance the carrier transport and consequently improve the device performance.^[26–28]

To further understand the influence of ODADI on PbI_2 and perovskite film formation, Fourier-transform infrared (FTIR) spectroscopy was used to study the interaction between ODADI and PbI_2 . The FTIR spectra of ODADI, ODADI PbI_2 , and PbI_2 thin films on SnO_2 substrates are shown in Figure 1c. As shown in Figure 1c, there are still ODADI contents even after the PbI_2 film coverage. Moreover, the existence of ODADI can be observed from the spectral features of N–H stretching at 1640–1560 cm^{-1} . N–H in ODADI shows a typical stretching vibration mode at 1594 cm^{-1} , while the upshifts to 1635 cm^{-1} in ODADI PbI_2 , demonstrate a strong interaction between NH_3^+ in ODADI and undercoordinated Pb^{2+} ions.^[29] Moreover, the interaction between ODADI and PbI_2 inhibits the formation of the compact PbI_2 layer, thus providing a favorable environment for organic salts diffusion. With this modified diffusion pathway, the growth of the perovskite film can be modulated. The fast growth of perovskite leads to small grains on the modified film and much finer grains are formed at the grain boundaries. Nevertheless, the small grain sizes and more grain boundaries will not impede the device performance when the defect states at grain boundaries and interfaces are well passivated with the ODADI molecules.^[30,31]

To determine the chemical composition of perovskite film and better understand the interaction between ODADI and perovskite, X-ray photoelectron spectroscopy (XPS) was performed. The XPS full spectrum exhibits characteristic peaks of Pb, I, O, and Cl, and in the control film, where the characteristic peaks of N are not prominent. However, the characteristic peaks of N are relatively obvious in the case of the ODADI-modified film (Figure S5 Supporting Information). It can be observed that there are residual ODADI at the grain boundaries and at the interfaces of perovskite films. The Pb 4f XPS core spectra correspond to perovskite films with and without ODADI, as depicted in Figure 1d. The Pb 4f peaks of control film are consistent with

the reported binding energies of constituent elements of perovskite material, where Pb 4f_{5/2} and Pb 4f_{7/2} peaks are 142.9 and 138.0 eV, respectively.^[26] In the case of Pb 4f_{5/2} and Pb 4f_{7/2} of ODADI-modified perovskite film, the peaks are 143.1 and 138.2 eV, respectively. The Pb 4f signal peaks shift to higher binding energy after ODADI modification, due to the interaction between ODADI and under-coordinated Pb^{2+} , which consequently affects the surrounding electronic cloud density of Pb^{2+} ions.^[32,33] In addition, there are two extra peaks at about 136.3 and 141.2 eV in Pb 4f spectra, which can be identified as metallic Pb species. Previous studies have demonstrated that this kind of metallic Pb serves as a notorious nonradiative recombination center, which is harmful to device performance.^[34] In this case, the much weaker Pb^0 peak intensity derived from the ODADI-modified perovskite film indicates a suppressed nonradiative recombination.

To investigate the interfacial charge transfer in perovskite films with and without ODADI molecules, a series of spectroscopy probes were used to determine their electronic properties. The energy band of perovskite films with and without ODADI was studied using ultraviolet photoelectron spectroscopy (UPS). As shown in Figure 2a, the work function (WF) of perovskite can be derived from the subtraction of UPS photoemission cutoff energy boundary ($E_{\text{cut-off}}$) of 21.22 eV.^[35] The E_{cutoff} values are 16.92 and 16.83 eV for the control film and ODADI-modified perovskite film, respectively. The WF is significantly dropped from 4.39 eV (control film) to 4.30 eV for ODADI-modified perovskite film. The ionization energy (IE) values are 5.96 and 5.87 eV for the control film and ODADI-modified perovskite film according to equation $\text{IE} = 21.22 [E_{\text{cut-off}} - E_{\text{onset}}]$. Their energy level is shown in Figure 2b.

Moreover, scanning Kelvin probe microscopy (SKPM) was performed to test the surface potential of perovskite film and the results are shown in Figure 2c,d. Their line-cut profiles, extracted from the measured SKPM mappings, are shown in Figure S6, Supporting Information, where the average surface potential of the control film is 358.2 mV, while the ODADI-modified film is 612.2 mV. The SKPM results are in line with the UPS due to a lower surface potential, corresponding to a higher WF. A larger surface potential of the ODADI-modified film is found which is about 254 mV larger than that of the control film. This signifies a larger built-in potential that leads to a stronger electron separation capacity toward SnO_2 .^[36]

To further analyze the charge transfer dynamics of perovskite/ SnO_2 with and without ODADI, photoluminescence (PL) and time-resolved PL (TRPL) measurements were performed, and the results are shown in Figure 2e,f, respectively. The PL intensity of perovskite film with ODADI modification is about two times higher than the control film, which suggests that SnO_2 can effectively extract electrons from the perovskite layer. Moreover, after ODADI treatment, a blueshift from 815 to 806 nm is observed in the PL peak. This blueshift in the PL peak also suggests that ODADI removes trap states due to the passivation of iodine vacancy defects.^[37] In addition, we tried to test low-power PL from glass side and perovskite side separately and found that the intensity of the emission peaks is different. As shown in Figure S7, Supporting Information, the PL intensity derived from glass side is higher than that from the perovskite side, which is mainly attributed to the fact that the bottom-located

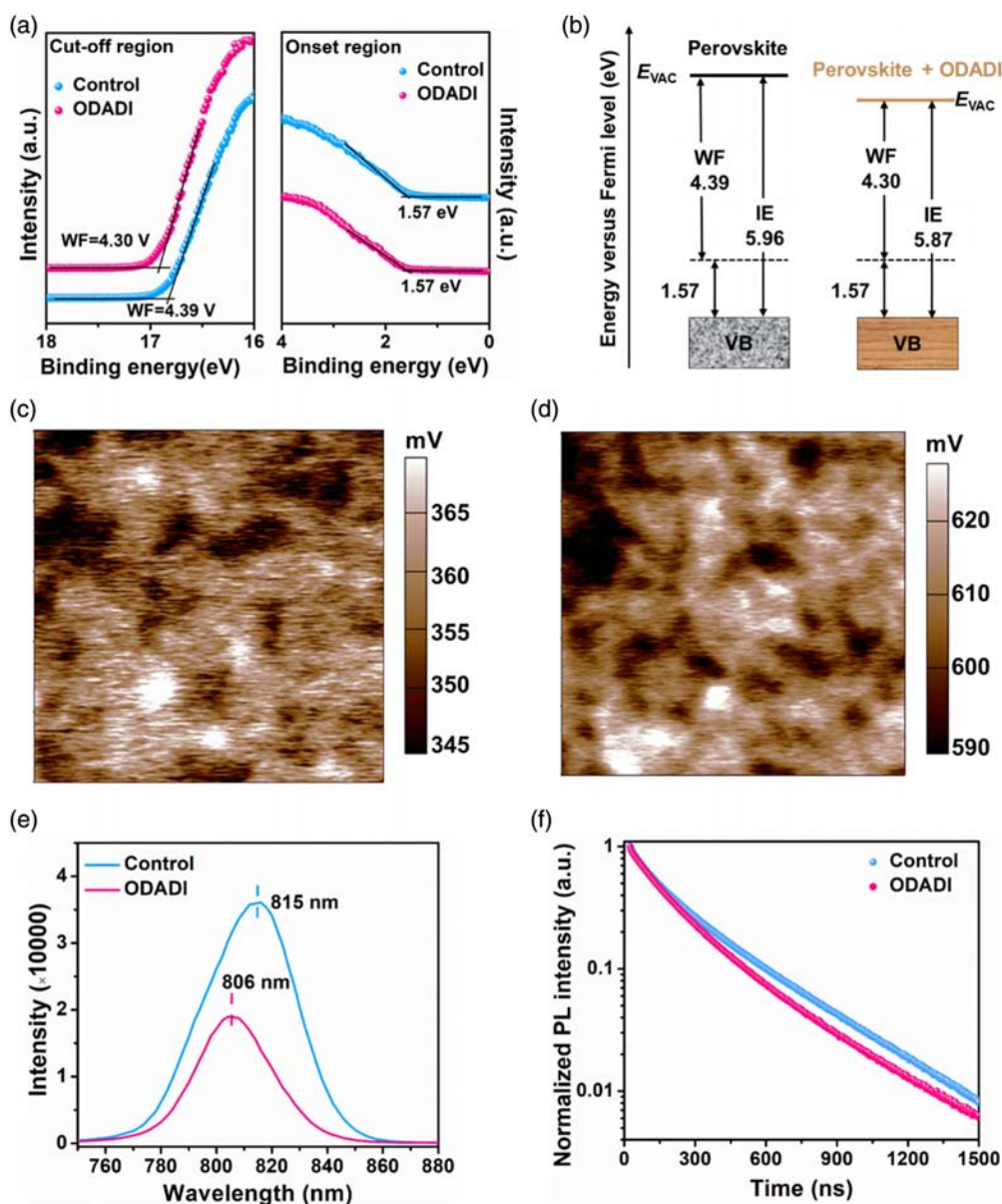


Figure 2. a) UPS and b) energy-level alignment of control and ODADI-modified perovskite films. SKPM mappings of perovskite films c) without and d) with ODADI. e) PL and f) TRPL of perovskite films without and with ODADI.

ODADI layer can passivate the defects at the perovskite/ETL interface.^[38] To quantify the charge transfer process, TRPL spectra are observed and fit by biexponential decay function $I(t) = A_1 \exp(-t/\tau_1) + A_2 \exp(-t/\tau_2)$ (Figure 2f). As summarized in Table S1, Supporting Information, the average lifetime (τ_{av}) of the ODADI-modified perovskite (239.8 ns) on ITO/SnO₂ is much shorter than that of the control film (277.9 ns), indicating that ODADI modification improves electron extraction, thus enhancing device efficiency.^[39,40]

To confirm the effectiveness of ODADI modification on device efficiency, PSCs based on different perovskite films with a planar architecture of ITO/SnO₂/ODADI/perovskite/spiro-OMeTAD/Au were fabricated. The schematic illustration of the device

structure is shown in Figure 3a. To reveal the detailed structure of the cross section of devices, scanning transmission electron microscopy (STEM) was performed. As shown in Figure 3b,c, individual functional layers of both control and ODADI-modified devices can be clearly distinguished. Au and Sn can be clearly observed from the elemental mappings, as shown in Figure S8, Supporting Information. In addition, Pb and I are distributed homogeneously throughout the entire perovskite films. Due to the influence of neighbor elements, the signal of N has considerable background noise. Nevertheless, it is clear that the ODADI-modified device has a brighter N signal between perovskite and SnO₂ than that of the control device, suggesting that ODADI molecules exist at the grain boundaries of the

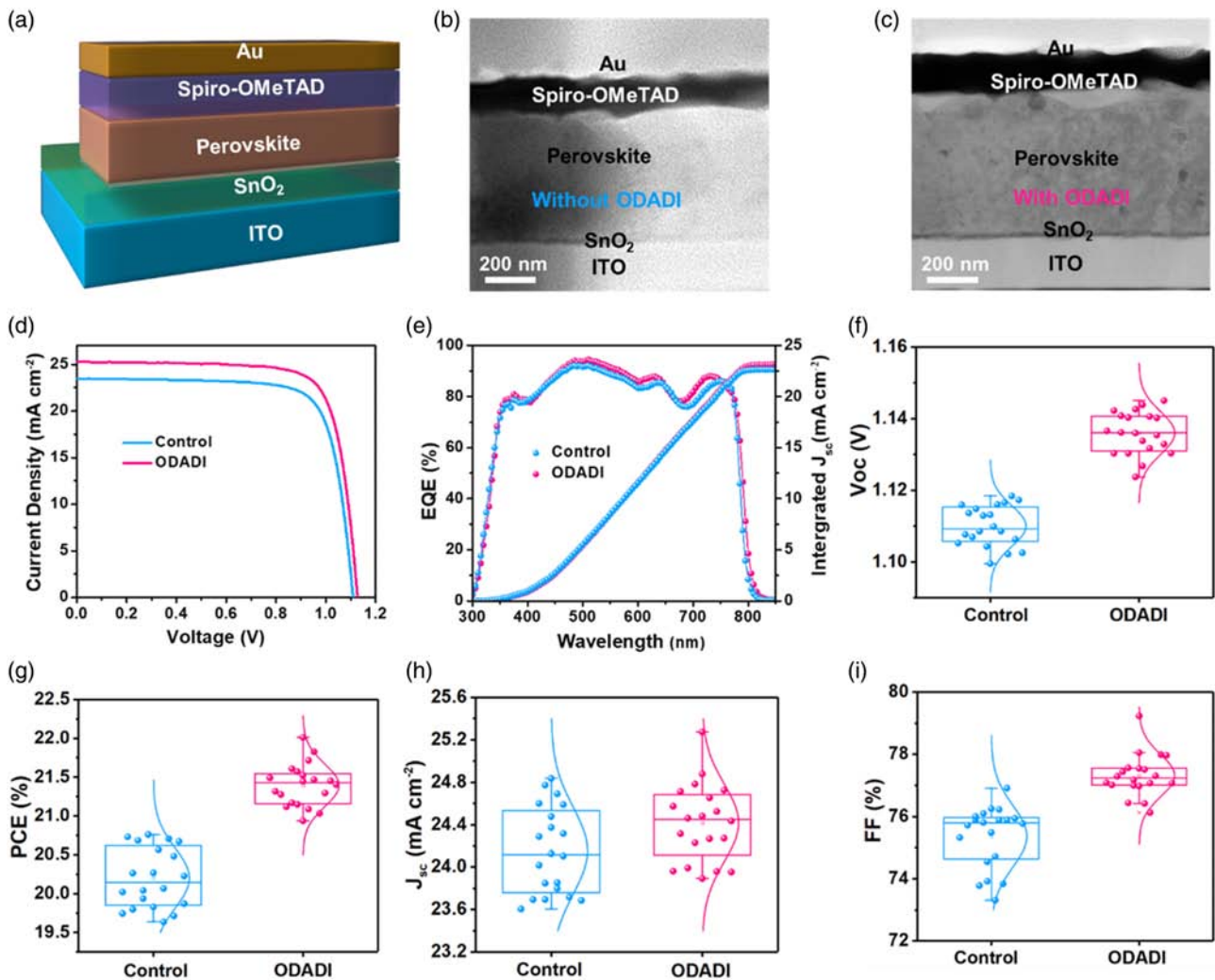


Figure 3. a) Schematic structure of the device. STEM of b) control and c) ODADI-modified device. d) $J-V$ curves and e) EQE and integrated J_{sc} curves of PSCs with and without ODADI. PSCs' statistics of f) PCE, g) V_{oc} , h) J_{sc} , and i) fill factor.

perovskite layer and the interface of the perovskite/ETL layer, which is in line with the SEM, FTIR, and XPS analysis.

Current density–voltage ($J-V$) curves of the champion PSCs based on perovskite films with and without ODADI are shown in Figure 3d. The detailed photovoltaic parameters are listed in Table S2, Supporting Information. It is clear that ODADI-based device yields a much larger V_{oc} (1.13 V) than its control counterpart (1.10 V), which is mainly attributed to the defect passivation introduced by ODADI. In addition, an enhancement on J_{sc} was observed as well due to the improved charge carrier extraction as discussed earlier (Figure 2f). With the more favorable V_{oc} and J_{sc} , a champion device with a PCE as high as 22.07% is achieved for the ODADI-based device, which is much higher than control device (19.87%). The external quantum efficiency (EQE) spectra are shown in Figure 3e. The corresponding integrated current densities are calculated to be 22.60 and 23.13 mA cm^{-2} for the control and ODADI-modified devices, respectively, which are consistent with the measured value. In addition, maximum power point (MPP) output was recorded with a bias of V_{MPP} , and the

results are presented in Figure S9, Supporting Information. It can be seen that the control and ODADI-based devices show steady-state current density at 23.3 and 23.8 mA cm^{-2} , leading to PCEs at 20.3 and 21.3%, respectively. The results are in agreement with the $J-V$ curves, indicating the reliability of the measured value. Figure 3f–i shows the statistical results of photovoltaic parameters derived from 20 independent devices based on different perovskite films. The narrower distributions of PCEs for ODADI-based devices suggest that ODADI modification contributes to better reproducibility, which is essential for further commercial application.

To characterize the passivation of trap-state density, space charge-limited current (SCLC) measurements of electron-only devices with a structure of ITO/SnO₂/with or without ODADI/perovskite/PC₆₁BM/Zracc/Ag are carried out. The $J-V$ curves are shown in Figure 4a, where the trap-filled limited voltage (V_{TFL}) can be obtained from the intersection of linear fits of the ohmic regime and the SCLC regime.^[41] According to the equation $N_{\text{trap}} = 2\epsilon_0\epsilon_r V_{TFL}/eL^2$, the trap-state density (N_{trap}) can be

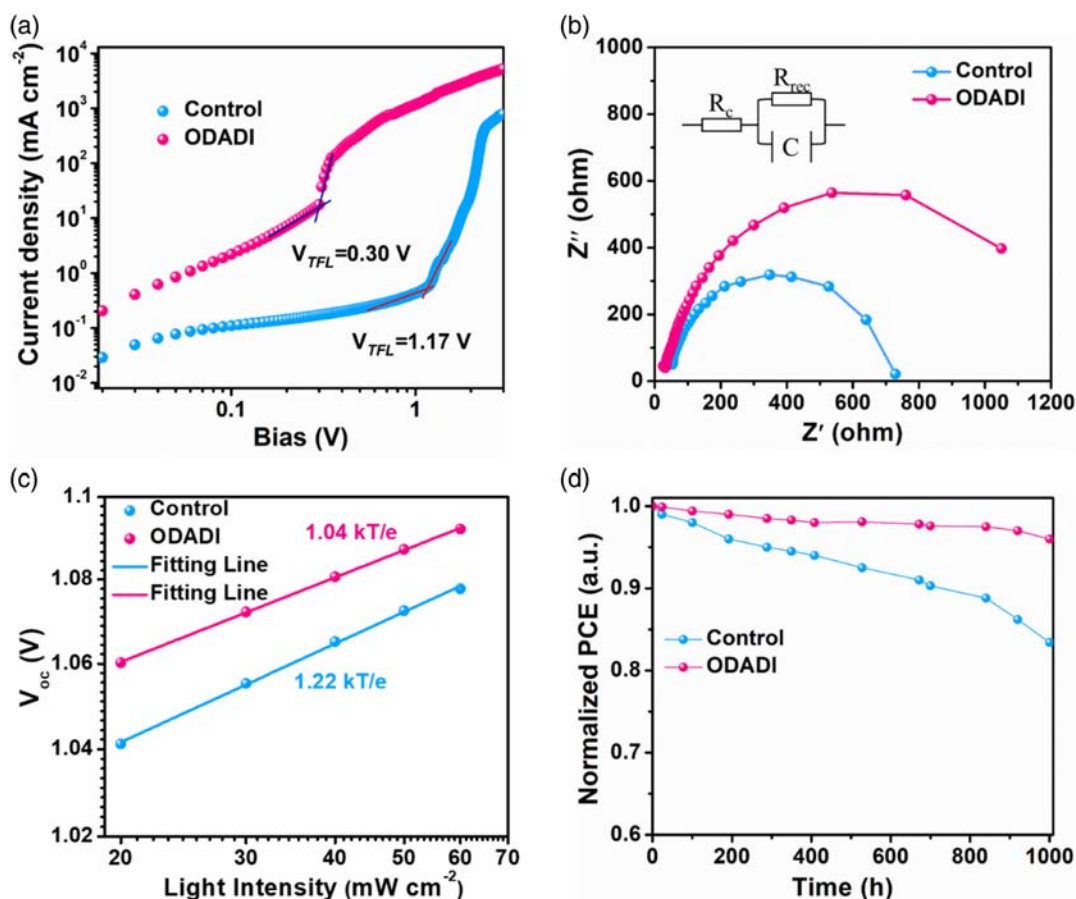


Figure 4. a) $J-V$ characteristics of the control and ODADI-modified electron-only devices, utilized for the estimation of defect density of the cells. b) EIS Nyquist plots of PSCs with and without ODADI. c) V_{oc} of the control and ODADI-modified PSCs, under different light intensities, together with their linear fits (solid lines). The axes were shown in logarithmic form. d) Stability measurements.

estimated from the trap-filled limit voltage (V_{TFL}), where ϵ_0 and ϵ_r are the vacuum permittivity and relative permittivity of perovskite, respectively, e is the elementary charge constant, and L is the thickness of perovskite film, which is around 500 nm according to Figure 3b,c.^[42] The V_{TFL} values of control and ODADI-modified devices are 1.17 and 0.3 V, respectively, and thus the trap-state density is reduced from 3.98×10^{16} to $1.02 \times 10^{16} \text{ cm}^{-3}$.

The device trap state density is strongly related to the carrier transport and recombination, which is also consistent with electrochemical impedance spectroscopy (EIS) measurements, as shown in Figure 4b. The inset shows the equivalent circuit that contains a charge transport resistance (R_c) and a charge recombination resistance (R_{rec}). The ODADI-modified perovskite-based device shows a larger semicircle which normally represents the recombination resistance. In this case, the larger semicircle suggests a suppressed nonradiative recombination process within the ODADI-based device, contributing to enhancement of V_{oc} .^[43,44] Figure 4c shows the V_{oc} versus light intensity, in which the deviation of slope from unity kT/q (where k is the Boltzmann constant, T represents the absolute temperature, and q denotes the elementary charge) indicates the recombination process.^[45–47] Therefore, the smaller slope of 1.04 kT q^{-1} derived from ODADI-based device suggests that the nonradiative

recombination process was effectively suppressed, leading to enhancement of device performance.

Finally, the storage stability of the unencapsulated photovoltaic devices is measured in a glove box (temperature of 25–30 °C). As depicted in Figure 4d, the ODADI-modified device still has 96% of the initial efficiency, while that of the control device can only keep 83% after 1000 h track. It is reported that the defect sites shorten the lifetime of perovskite devices. The reason behind this is defect-induced degradation.^[48,49] In addition, thermal stability of the devices was evaluated by collecting the $J-V$ curves at 85 °C for 800 h (Figure S10, Supporting Information). It is noted that the PCE of the control device decreased to 61% of its initial PCE, while the ODADI-modified device still maintains 90% of its original value. This significant thermal stability enhancement is attributed to the improved interfacial contact and defect passivation induced by ODADI modification.

3. Conclusion

In summary, ODADI-based alkylammonium predeposition strategy was developed to fabricate the high-quality perovskite film via a two-step method. The predeposited ODADI molecules not

only improve the growth of perovskite film but also passivate the buried-interface defects. The resulting perovskite film shows improved crystallinity, prolonged carrier lifetime, reduced defect density, and enhanced charge carrier extraction. As a result, an enhancement of device efficiency from 19.87% to 22.07% was achieved. In addition, it is found that the introduction of ODADI can significantly enhance the long-term as well as thermal stability due to the buried-interface defect passivation. Therefore, it is believed that the proposed alkylammonium predeposition strategy can be widely adopted to modulate buried interface, thus showing great potential toward highly performed two-step-processed PSCs.

Supporting Information

Supporting Information is available from the Wiley Online Library or from the author.

Acknowledgements

H.L., X.Q., and J.W. contributed equally to this work. The authors thank all the funding support from the National Key Research and Development Program of China (2018YFB0704100), Key-Area Research and Development Program of Guangdong Province (2019B010941001), and the Leading talents of Guangdong Province Program (2016LJ06N507).

Conflict of Interest

The authors declare no conflict of interest.

Data Availability Statement

The data that support the findings of this study are available from the corresponding authors upon reasonable request.

Keywords

alkylammonium, high performances, passivations, perovskite solar cells

Received: November 12, 2021

Revised: December 19, 2021

Published online: January 19, 2022

- [1] A. Kojima, K. Teshima, Y. Shirai, T. Miyasaka, *J. Am. Chem. Soc.* **2009**, *131*, 6050.
- [2] E. M. Tennyson, T. A. S. Doherty, S. D. Stranks, *Nat. Rev. Mater.* **2019**, *4*, 573.
- [3] D. Zhao, C. Chen, C. Wang, M. M. Junda, Z. Song, C. R. Grice, Y. Yu, C. Li, B. Subedi, N. J. Podraza, X. Zhao, G. Fang, R.-G. Xiong, K. Zhu, Y. Yan, *Nat. Energy* **2018**, *3*, 1093.
- [4] C. Wehrenfennig, G. E. Eperon, M. B. Johnston, H. J. Snaith, L. M. Herz, *Adv. Mater.* **2014**, *26*, 1584.
- [5] M. A. Green, A. Ho-Baillie, H. J. Snaith, *Nat. Photonics* **2014**, *8*, 506.
- [6] National Renewable Energy Laboratory (NREL), Research Cell Efficiency Records, <https://www.nrel.gov/pv/assets/pdfs/pv-efficiency-chart.png> (accessed: November 2021).
- [7] S. Pu, J. Fu, Y. Liao, L. Ge, Y. Zhou, S. Zhang, S. Zhao, X. Liu, X. Hu, K. Liu, J. Chen, *Adv. Mater.* **2020**, *32*, 1907307.
- [8] J. Ramanujam, U. P. Singh, *Energy Environ. Sci.* **2017**, *10*, 1306.
- [9] T. A. M. Fiducia, B. G. Mendis, K. Li, C. R. M. Grovenor, A. H. Munshi, K. Barth, W. S. Sampath, L. D. Wright, A. Abbas, J. W. Bowers, J. M. Walls, *Nat. Energy* **2019**, *4*, 504.
- [10] Z. Xiao, C. Bi, Y. Shao, Q. Dong, Q. Wang, Y. Yuan, C. Wang, Y. Gao, J. Huang, *Energy Environ. Sci.* **2014**, *7*, 2619.
- [11] J. H. Im, I. H. Jang, N. Pellet, M. Gratzel, N. G. Park, *Nat. Nanotechnol.* **2014**, *9*, 927.
- [12] J. Burschka, N. Pellet, S. J. Moon, R. Humphry-Baker, P. Gao, M. K. Nazeeruddin, M. Gratzel, *Nature* **2013**, *499*, 316.
- [13] P. Shi, Y. Ding, Y. Ren, X. Shi, Z. Arain, C. Liu, X. Liu, M. Cai, G. Cao, M. K. Nazeeruddin, S. Dai, *Adv. Sci.* **2019**, *6*, 1901591.
- [14] X. Zheng, B. Chen, J. Dai, Y. Fang, Y. Bai, Y. Lin, H. Wei, Xiao C. Zeng, J. Huang, *Nat. Energy* **2017**, *2*, 17102.
- [15] Y. Deng, E. Peng, Y. Shao, Z. Xiao, Q. Dong, J. Huang, *Energy Environ. Sci.* **2015**, *8*, 1544.
- [16] B. Chen, H. Chen, Y. Hou, J. Xu, S. Teale, K. Bertens, H. Chen, A. Proppe, Q. Zhou, D. Yu, K. Xu, M. Vafaei, Y. Liu, Y. Dong, E. H. Jung, C. Zheng, T. Zhu, Z. Ning, E. H. Sargent, *Adv. Mater.* **2021**, *33*, 2103394.
- [17] Q. Jiang, L. Zhang, H. Wang, X. Yang, J. Meng, H. Liu, Z. Yin, J. Wu, X. Zhang, J. You, *Nat. Energy* **2016**, *2*, 16177.
- [18] X. Zheng, J. Troughton, N. Gasparini, Y. Lin, M. Wei, Y. Hou, J. Liu, K. Song, Z. Chen, C. Yang, B. Turedi, A. Y. Alsalloum, J. Pan, J. Chen, A. A. Zhumekenov, T. D. Anthopoulos, Y. Han, D. Baran, O. F. Mohammed, E. H. Sargent, O. M. Bakr, *Joule* **2019**, *3*, 1963.
- [19] D. Bi, C. Yi, J. Luo, J.-D. Décoppet, F. Zhang, S. M. Zakeeruddin, X. Li, A. Hagfeldt, M. Grätzel, *Nat. Energy* **2016**, *1*, 16142.
- [20] Z. Wang, Q. Lin, F. P. Chmiel, N. Sakai, L. M. Herz, H. J. Snaith, *Nat. Energy* **2017**, *2*, 17135.
- [21] Q. Jiang, Y. Zhao, X. Zhang, X. Yang, Y. Chen, Z. Chu, Q. Ye, X. Li, Z. Yin, J. You, *Nat. Photonics* **2019**, *13*, 460.
- [22] Q. Jiang, Z. Chu, P. Wang, X. Yang, H. Liu, Y. Wang, Z. Yin, J. Wu, J. You, *Adv. Mater.* **2017**, *29*, 1703852.
- [23] M. Qin, H. Xue, H. Zhang, H. Hu, K. Liu, Y. Li, Z. Qin, J. Ma, H. Zhu, K. J. A. M. Yan, S. Tao, X. Lu, *Adv. Mater.* **2020**, *32*, 2004630.
- [24] S. Wu, J. Zhang, Z. Li, D. Liu, M. Qin, S. H. Cheung, X. Lu, D. Lei, S. K. So, Z. Zhu, A. K. Y. Jen, *Joule* **2020**, *4*, 1248.
- [25] X. Zheng, Y. Hou, C. Bao, J. Yin, F. Yuan, Z. Huang, K. Song, J. Liu, J. Troughton, N. Gasparini, C. Zhou, E. H. Sargent, O. M. Bakr, *Nat. Energy* **2020**, *5*, 131.
- [26] W. Q. Wu, J. X. Zhong, J. F. Liao, C. Zhang, Y. Zhou, W. Feng, L. Ding, L. Wang, D.-B. Kuang, *Nano Energy* **2020**, *75*, 104929.
- [27] S. Draguta, O. Sharia, S. J. Yoon, M. C. Brennan, Y. V. Morozov, J. S. Manser, P. V. Kamat, W. F. Schneider, M. Kuno, *Nat. Commun.* **2017**, *8*, 200.
- [28] M. C. Brennan, S. Draguta, P. V. Kamat, M. Kuno, *ACS Energy Lett.* **2017**, *3*, 204.
- [29] R. Wang, J. Xue, K.-L. Wang, Z.-K. Wang, Y. Luo, D. Fenning, G. Xu, S. Nuryyeva, T. Huang, Y. J. S. Zhao, *Science* **2019**, *366*, 1509.
- [30] J. Liang, P. Zhao, C. Wang, Y. Wang, Y. Hu, G. Zhu, L. Ma, J. Liu, Z. Jin, *J. Am. Chem. Soc.* **2017**, *139*, 14009.
- [31] H. Xiao, T. Liang, M. Xu, *Small* **2019**, *15*, 1901767.
- [32] G. Sadoughi, D. E. Starr, E. Handick, S. D. Stranks, M. Gorgoi, R. G. Wilks, M. Bär, H. J. Snaith, *ACS Appl. Mater. Interfaces* **2015**, *7*, 13440.
- [33] J. Liang, Z. Liu, L. Qiu, Z. Hawash, L. Meng, Z. Wu, Y. Jiang, L. K. Ono, Y. Qi, *Adv. Energy Mater.* **2018**, *8*, 1800504.
- [34] W. Zhu, Q. Zhang, D. Chen, Z. Zhang, Z. Lin, J. Chang, J. Zhang, C. Zhang, Y. Hao, *Adv. Energy Mater.* **2018**, *8*, 1802080.
- [35] W. Zhu, Z. Zhang, W. Chai, Q. Zhang, D. Chen, Z. Lin, J. Chang, J. Zhang, C. Zhang, Y. Hao, *ChemSusChem* **2019**, *12*, 2318.

- [36] Y. Wu, W. Chen, Y. Lin, B. Tu, X. Lan, Z. Wu, R. Liu, A. B. Djurišić, Z. B. He, *ACS Appl. Energy Mater.* **2018**, *1*, 3984.
- [37] Y. Shao, Z. Xiao, C. Bi, Y. Yuan, J. Huang, *Nat. Commun.* **2014**, *5*, 5784.
- [38] J. Z. Chen, X. Zhao, S. G. Kim, N. G. Park, *Adv. Mater.* **2019**, *31*, 1902902.
- [39] Q. Han, Y. Bai, J. Liu, K.-Z. Du, T. Li, D. Ji, Y. Zhou, C. Cao, D. Shin, J. Ding, A. D. Franklin, J. T. Glass, J. Hu, M. J. Therien, J. Liu, D. B. Mitzi, *Energy Environ. Sci.* **2017**, *10*, 2365.
- [40] J. Peng, J. I. Khan, W. Liu, E. Ugur, T. Duong, Y. Wu, H. Shen, K. Wang, H. Dang, E. Aydin, X. Yang, Y. Wan, K. J. Weber, K. R. Catchpole, F. Laquai, S. Wolf, T. P. White, *Adv. Energy Mater.* **2018**, *8*, 1801208.
- [41] D. Shi, V. Adinolfi, R. Comin, M. Yuan, E. Alarousu, A. Buin, Y. Chen, S. Hoogland, A. Rothenberger, K. J. S. Katsiev, *Science* **2015**, *347*, 519.
- [42] S. Fu, W. Zhang, X. Li, L. Wan, Y. Wu, L. Chen, X. Liu, J. Fang, *ACS Energy Lett.* **2020**, *5*, 676.
- [43] A. R. Pascoe, N. W. Duffy, A. D. Scully, F. Huang, Y.-B. Cheng, *J. Phys. Chem. C.* **2015**, *119*, 4444.
- [44] F. Yang, H. E. Lim, F. Wang, M. Ozaki, A. Shimazaki, J. Liu, N. B. Mohamed, K. Shinokita, Y. Miyauchi, A. Wakamiya, Y. Murata, K. Matsuda, *Adv. Mater. Interfaces* **2017**, *5*, 1701256.
- [45] X. Shi, R. Chen, T. Jjiang, S. Ma, X. Liu, Y. Ding, M. Cai, J. Wu, S. Dai, *Sol. RRL* **2019**, *4*, 1900198.
- [46] N. Li, S. Tao, Y. Chen, X. Niu, C. K. Onwudinanti, C. Hu, Z. Qiu, Z. Xu, G. Zheng, L. Wang, Y. Zhang, L. Li, H. Liu, Y. Lun, J. Hong, X. Wang, Y. Liu, H. Xie, Y. Gao, Y. Bai, S. Yang, G. Brocks, Q. Chen, H. Zhou, *Nat. Energy* **2019**, *4*, 408.
- [47] M. Zhang, X. Cui, Y. Wang, B. Wang, M. Ye, W. Wang, C. Ma, Z. Lin, *Nano Energy* **2020**, *71*, 104620.
- [48] M. Chen, M. G. Ju, H. F. Garces, A. D. Carl, L. K. Ono, Z. Hawash, Y. Zhang, T. Shen, Y. Qi, R. L. Grimm, D. Pacifici, X. C. Zeng, Y. Zhou, N. P. Padture, *Nat. Commun.* **2019**, *10*, 16.
- [49] B. Wang, M. Zhang, X. Cui, Z. Wang, M. Rager, Y. Yang, Z. Zou, Z. L. Wang, Z. Lin, *Angew. Chem. Int. Ed.* **2020**, *59*, 1611.